Published in final edited form as:
Int J Mass Spectrom. 2011 June 1; 303(2-3): 191–198. doi:10.1016/j.ijms.2011.02.003.

Biologically Relevant Metal-Cation Binding Induces Conformational Changes in Heparin Oligosaccharides as Measured by Ion Mobility Mass Spectrometry

Youjin Seo[a], **Matthew R. Schenauer**[b], and **Julie A. Leary**[a]

[a] Departments of Chemistry and Molecular and Cellular Biology, University of California, Davis, CA 95616, USA

[b] Amgen Inc., One Amgen Center Drive, Thousand Oaks, CA 91320, USA

Abstract

Heparin interacts with many proteins and is involved in biological processes such as anticoagulation, angiogenesis, and antitumorigenic activities. These heparin-protein interactions can be influenced by the binding of various metal ions to these complexes. In particular, physiologically relevant metal cations influence heparin-protein conformations through electronic interactions inherent to this polyanion. In this study, we employed ion mobility mass spectrometry (IMMS) to observe conformational changes that occur in fully-sulfated heparin octasaccharides after the successive addition of metal ions. Our results indicate that binding of positive counter ions causes a decrease in collision cross section (CCS) measurements, thus promoting a more compact octasaccharide structure.

Introduction

Heparin is a commercially-available pharmaceutical drug typically administered as an anticoagulant [1], and exists as a highly sulfated glycosaminoglycan (GAG) found in the granules of mast cells [2, 3]. It is composed of repeating disaccharide units of hexuronic acid (L-iduronic acid or its C-5 epimer, D-glucuronic acid) linked (α1→ 4) to D-glucosamine[4]. Sulfation can occur at the 6-O- and/or N-positions of glucosamine as well as the 2-O position of the hexuronic acid [5]. Previous studies have established that 2-O-sulfated L-iduronic acid exists in equilibrium between the chair ($^1C_4$) and skew boat ($^2S_0$) conformations [6–9].

Various substitution patterns of carbohydrate residues affect the conformation around glycosidic linkages[10]. Importantly, the flexibility of various hexuronic acid conformations depends on adjacent sulfated residues, surrounding counter ions, and /or water [11, 12]. A relationship exists between the biological activity of heparin and the structure of a heparin:protein complex [5, 13, 14]. A classic example of this is in the blood-coagulation cascade where the interaction of antithrombin with Arixtra (a heparin pentasaccaharide analog) causes an alteration in conformation of antithrombin, thus inhibiting factor Xa, a coagulation proteinase [15, 16].

The effect of metal ions on protein-carbohydrate complexes and their biological activities is largely unknown. Some studies have reported that physiological metal ions such as sodium, calcium, and magnesium bind to heparin based on the polyelectrolyte theory [17–20]. In addition, there is increasing evidence that divalent metal ions (Ca^{2+}, Cu^{2+}, and Zn^{2+}) are necessary in many protein-heparin interactions thus influencing the affinity [18, 21–23], specificity [24, 25] and stability [26–28] of these complexes. Conformational changes of heparin induced by calcium ions are necessary for the interaction between the anticoagulant heparin and annexin V [18]. Therefore, the investigation of the conformational changes of heparin caused from the binding to metal ions may be a significant step towards understanding the biological properties of protein-heparin complexes.

To address the physicochemical properties involved in metal ion binding to heparin, many researchers have employed different spectroscopic methods such as IR [29, 30], NMR [10, 11, 20, 25, 31–33], circular dichroism [34–37], and synchrotron radiation circular dichroism [38, 39]. These methods were applied to study specific or non-specific binding of heparin to metal ions and were used to measure conformational changes around either the uronic acid residues or the glycosidic bonds.

In addition to spectroscopy, ion mobility mass spectrometry (IMMS) has recently emerged on the forefront of conformation analysis, and has been used in the investigations of small molecules and protein conformations in the gas phase by directly measuring their collision cross sections (CCS) [40–44]. Several groups have shown that conformations in the gas phase are consistent with measurements made using solution and/or solid structures [44–51]. IMMS methods have been established for studying oligosaccharides as this technique has the capability to separate the various isomers [52–55]. Additionally, IMMS can be used to obtain structural information on sodiated carbohydrates [49, 56] and glycans [57]. In our experiments, we employ nano-electrospray coupled with quadrupole-traveling wave ion mobility time of flight mass spectrometry to probe conformational changes of metal ion coordinated heparin.

We have chosen to fully interrogate sulfated heparin octasaccharides in our study. Heparin octasaccharides are required for antithrombin binding and thus serve as anticoagulants [58–60]. They also inhibit the angiogenic properties of cytokine fibroblast growth factor-2 [61], and are critical during inflammation as they are involved in the dimerization of monocyte chemoattractant protein-1 [62, 63].

Herein, we report the conformational changes of heparin octasaccharide bound to a series of physiologically relevant metal ions (Na^+, K^+, Mg^{2+}, Ca^{2+}). Additionally, we have examined the impact of transition metal ion (Mn^{2+}, Co^{2+}, Fe^{2+}, Ni^{2+}) binding on the overall shape of the heparin octasaccharide. On the basis of these observations, our data indicate that not only does each metal ion independently have an effect on the conformational change of heparin octasaccharide based on ionic radii and valence of cations, but the number of metal ion adducts also has an effect on the overall structure of metal ion coordinated heparin octasaccharide.

EXPERIMENTAL SECTION

Materials

Heparin octasaccharide was purchased from V-labs, INC (Covington, LA). Ni $(OAc)_2 \cdot 4H_2O$ and $FeCl_2 \cdot 4H_2O$ were purchased from Sigma-Aldrich Corp. (St. Louis, MO). $CoCl_2 \cdot 6H_2O$ and $MnCl_2 \cdot H_2O$ were purchased from Fisher Scientific (Fair Lawn, NJ) and Mallinckrodt (Paris, KY), respectively. Oligonucleotides TTTTTTT (T7), CCCCCCC (C7), and ATATAT ($(AT)_3$) were purchased from Invitrogen (Carlsbad, CA). The IonPac AS7 anion

exchange column was purchased from Dionex (Sunnyvale, CA). All solutions were of HPLC grade and purchased from Sigma-Aldrich Corp. (St. Louis, MO).

Preparation of metal coordinated heparin octasaccharides

Heparin octasaccharides were separated by strong anion exchange chromatography (SAX) to obtain only dodecasulfated species as previously described[64]. Briefly, SAX chromatography was performed on a Waters Delta 600 system (Waters Corp., Milford, MA) using the IonPac AS7 Column (4.00×250mm). The separation was optimized by linear gradient elution with solution A, 4M NaCl (pH 3.7), and solution B, H_2O (pH 3.7) to isolate the octasaccharides according to sulfate group content as follows: 0–12% A, 0–15min; 12–60% A, 15min–60min. Each elution peak was detected by a UV-VIS spectrophotometer set at 232nm, and the dodecasulfated heparin octasaccharides were collected. The fractions were then applied to a 1KDa molecular weight cut off (MWCO) Dispo-Biodilazer (The Nest Group Inc., Southborough MA) for desalting at room temperature. The concentration of the desalted sample was determined by UV-VIS spectrometry with $\varepsilon=5500 M^{-1}cm^{-1}$ in 30mM HCl at 232nm. Metal bound dodecasulfated heparin octasaccharides were prepared at an optimum concentration ratio of carbohydrate and metal salt (1:100) in 1:1(v/v) MeOH: 2% acetic acid aqueous solution. Metal ion solutions of Ca^+ and K^+ were analyzed prior to use to ensure purity.

IMS-MS of metal coordinated dodecasulfated heparin octasaccharide

Ion mobility mass spectrometry analysis was performed on the Synapt HDMS system (Waters Corp., Milford, MA) with nano-electrospray ionization. The samples were infused using in- house prepared capillaries in the negative ionization mode with a capillary voltage of 0.7kV [64]. The TOF mass analyzer was calibrated using sodium formate in 1:1(v:v) acetonitrile: H_2O from 50 to 1000 m/z to obtain mass accuracy within 3ppm. The Synapt parameters were optimized as following parameters: the sample cone voltage and extraction cone voltage were set at 5V and 0.5V, respectively, the trap collision energy was set at 1V, and transfer collision energy was set at 2.5V. Low voltages in the collision cell were chosen to avoid desulfation of dodecasulfated heparin octasaccharides. The trap T-wave cell was operated at a flow rate of 1.0mL/min. For optimal ion mobility separation, the traveling wave velocity and pulse height were set at 400m/s and 8.0V, respectively. The ion mobility cell was kept at a pressure of 0.5mbar of nitrogen. Arrival time distributions (ATDs) of ions were recorded for 9ms corresponding to a pusher period of 45μs in the TOF analyzer at a pressure of 1.02×10^{-6}mbar. Five independent data sets were acquired for each sample and were processed with MassLynx (V4.1) software.

Calibration curve for collision cross section measurements

A calibration curve was constructed using a mixture of 20μM T7, C7, and $(AT)_3$ in 10mM NH_4OH in 1:1(v:v) MeOH: H_2O under the same instrument parameters as previously described. For each oligonucleotide, individual charge state ions were identified and their ATDs reported. Since the Synapt HDMS system cannot directly obtain absolute collision cross sections from ATDs of ions (as compared with conventional IMS-MS[65]), absolute collision cross sections (CCS) of oligonucleotides were determined using conventional IMS-MS from the laboratory of Michael T. Bowers at the University of California, Santa Barbara. The CCS were calculated according to previously described protocols [41, 66]. Corrected CCS were required in order to account for charge state and reduced mass. Subsequently, the corrected ATDs of the oligonucleotides for each charge state were plotted against the corrected CCS. The calibration curve was fitted using a linear series. Corrected ATDs of individual metal coordinated heparin octasaccharides ions were converted from measured ATDs as described before. The CCS were determined by the formula derived from the linear

equation in the calibration curve and then corrected for charge state and reduced mass, as indicated in the equation below:

$$Y=43.10X+318.9 \text{ where } R^2=0.99$$

where Y is the corrected CCS of oligonucleotides and X is the corrected ATDs of oligonucleotides.

RESULT AND DISCUSSION

Mass spectrometry and ion mobility analysis of heparin octasaccharide

In this study, ion mobility mass spectrometry (IMMS) was used to investigate the conformational changes of heparin octasaccharide upon metal ion binding. We first observed the dodecasulfated heparin octasaccharide as a series of deprotonated ions, as well as sodium or potassium ion bound forms (Figure 1). Of particular interest is the observation that the 4^- and 5^- charge states predominate under these conditions. With the use of IMMS, we next investigated the arrival time distributions (ATDs) of the octasaccharide with and without adducted sodium ions. For either the 4^- or 5^- charge states, the general trend observed was that the arrival time (AT) was inversely proportional to the number of the sodium adducts; as the number of sodium adducts increased, the AT decreased (Figure 2). This phenomenon suggests that an increased number of bound sodium ions induces a more compact octasaccharide structure regardless of the increasing mass of the ion-bound octasaccharide. A possible explanation for the compact structure resulting from metal ion binding may be due to the fact that the 2-O-sulfur-L-iduronic acid units of the heparin octasaccharide are flexible [49, 67], and that the positively charged metal ions cause the flexible rings to encapsulate it, thereby creating a more compact structure. The metal ion may also coordinate to the 6-position sulfates, causing the oligosaccharide to form a multi-coordinated structure. Interestingly, the overall effects of compact structure formation are seen more dramatically in the 4^- than in the 5^- charge state. This may be explained by the fact that the charge-charge repulsion is stronger in the 5^- charge state than that of the 4^- charge state, thereby hindering the formation of the compact structure.

Effects of various metal ions on arrival time distributions (ATDs) of metal coordinated heparin octasaccharide

After investigating the effect of the sodium ion adduct on overall heparin octasaccharide compact structure formation, we next investigated the effects of other types of metal ions on the same octasaccharide. In addition to the alkali metal sodium, we also investigated the effects of the alkaline earth metals potassium and calcium, and the transition metal, nickel. All of these metal ions have been previously shown to have a biological effect on heparin [68–70], and therefore were reasonable candidates for examination. Despite the different properties of each metal ion adduct, the results mirrored that of sodium; increasing the number of metal adduct ions caused the formation of a more compact structure (Figure 3). Whether these compact structures are structurally similar to those induced by sodium is yet to be determined. However, various metal ion properties which include, but are not limited to, ionic radii, charge, coordination geometry, specificity for octasaccharide metal ion binding sites (O-sulfates, N-sulfates, or carboxylates), or ionic strengths, may all factor into the formation of the compact structure observed in the gas phase. Figure 3 shows that octasaccharides bound to calcium or nickel ions undergo larger differences in arrival times (ATs) between metal ion-bound and metal ion-free states compared to that of the sodium or potassium-bound ions. The maximum difference in ATDs was observed at 0.79msec for the 5^- charge state and 2.51 msec for the 4^- charge state. Divalent cations strongly draw

negatively charged groups of the octasaccharide to encapsulate it, thus generating a more compact structure. In addition, potassium coordinated octasaccharides show a larger decrease in ATs (0.49 msec in the 5^- charge state, 2.30 msec in the 4- charge state) than sodium coordinated (0.23 msec in the 5^- charge state, 2.00 msec in the 4^- charge state) despite the increased ionic radii of the potassium versus the sodium ion. This phenomenon suggests that ions with larger ionic radii induce a more complete enclosure by the octasaccharide, but ions with smaller ionic radii induce only a partial folding of the octasaccharide. Thus, potassium ions generate more compact structures than sodium ions. Similarly, the relatively large ionic radii of the potassium ion would likely have an effect of masking the negatively charged groups of the octasaccharide, thus lessening the charge-charge repulsion of closely-spaced negatively-charged groups.

Interestingly, the ATDs representing the 4^- charged potassium and calcium-coordinated octasaccharides are significantly different (Figure 4). Since potassium ions bind to heparin nonspecifically[19], there are two possible metal ion binding sites on the octasaccharide. One possible mode of binding would bring the reducing and the non-reducing rings close to each other to generate an overall compact structure. The other possibility suggests that two or more proximal sulfation sites of the octasaccharide coordinate to the potassium ion; i.e. two or more sulfates groups could simultaneously bind to the potassium ion[71–75]. However, without significant modeling studies, it would be very difficult if not impossible to ascertain which of these conformations predominates. The octasaccharide bound to one calcium ion generates a similarly compact structure to that of the potassium coordinated ion. Previous studies have shown that calcium ions bind more favorably in the region located between the glucosamine and iduronic residues of heparin hexasaccharide[25]. This observation suggests that a single calcium ion can bind either a favorable or unfavorable site of octasaccharide thus leading to two ion populations. (Figure 4b), right)

Collision cross section measurements of metal- coordinated heparin octasaccharide

From each measured ATD, we then calculated the corresponding collision cross sections (CCS) of octasaccharide bound to the various metal ion adducts. When calibrating the Synapt IMMS instrument to calculate CCS of the octasaccharide, there are two commonly used curves with which to fit the data; a power fit [76] and a linear fit[77]. Since previous studies showed that the linear fit was found to be the more appropriate method for small molecules[77], we used this method for analysis. Indeed, our data are consistent when using a linear fit method for calculating CCS of metal coordinated- and free- octasaccharide. The relationship between estimated cross sections and published cross sections of oligonucleotide standard mixture is best described by a linear relationship (R^2=0.9985, Figure 5).

The binding of successive metal ions to the octasaccharide results in a decreased CCS of the metal ion coordinated octasaccharide (Table 1a). There are no general differences observed in the calculated CCS of Na^+ adducted versus K^+ adducted octasaccharide when more than one metal ion is present. However, a 23 $Å^2$ difference is apparent for the single metal ion species; the single potassium ion promotes formation of two populations with different conformations. The increased number of metal ion adducts may bind more free sulfate groups or carboxylates that would otherwise experience charge-charge repulsion, thus generating a more compact conformational change compared to fewer metal ion adducts.

Next, we calculated the CCS of heparin bound to alkaline earth metal ions (Table 1b). As with alkali metals, similar trends were observed; the CCS of Mg^{2+} and Ca^{2+} did not vary significantly, except that one Ca^{2+} binding also produced two populations. In general, a cross comparison between the CCS of alkali and alkaline earth metals showed that alkaline earth metals impart a greater change in CCS than that of alkali metals. For the ions in

$1s^2 2s^2 2p^6$ configuration, the maximum differences were observed with 4 adducts with a difference of 11 $Å^2$ between 4 sodium coordination and 4 magnesium coordination. For the ions in $1s^2 2s^2 2p^6 3s^2 3p^6$ configuration, the maximum differences were observed with 3 adducts with a difference of 12 $Å^2$ occurring between the 3 potassium coordinated and the 3 calcium coordinated octasaccharides. The more compact structure generated by the alkaline earth metal ions may be explained by the stronger effective nuclear charge and/or by the fact that alkaline earth metal ions have higher charge densities than the alkali metal ions which therefore allow the negatively charged, highly sulfated oligomers to adopt a more compact structure.

Lastly, we investigated the effects of transition metal ions on collisional cross sections of heparin octasaccharide (Table 2). As with alkali metal and alkali earth metal ions, similar trends of decreased CCSs upon successive additions of metal ions were observed. However, the greatest difference observed for transition metal ions occurred at the singly metal ion bound form i.e. the cobalt adduct differed from one nickel adduct by 13$Å^2$ (Figure 6). Adding successive metal ions did not lead to a greater difference in CCS between each transition metal ion species. The observation suggests that the induced conformational change is not specific to any specific transition metal ion. The slightly different observed CCS of four transition metal coordinated octasaccharides are likely due to different ionic radii of the metal ions used in this study. Given the above data, under the conditions used in this study, it does not appear that the more compact structure depends on ionic radii or mass of the transition metal ion, e.g. cobalt. Several groups have reported that the conformation of protein bound to transition metal ion changes depending on spin states [78–80]. The cobalt ion in high spin has a larger ionic radius (89pm) than the same ion in a low-spin state (79pm). Cobalt ions bound to the octasaccharide appear to follow this general trend. This result also suggests that there are differences in the binding interactions of the cobalt ion and the octasaccharide depending on the spin state, thus having an effect on the overall conformational change.

Overall, our IMMS data demonstrate that various metal ions induce conformational changes when bound to the octasaccharide compared with those without metal ion coordination. Among the physiologically relevant cations (Na^+, K^+, Mg^{2+}, Ca^{2+}), calcium in particular has been shown to induce remarkable conformational changes in solution [20, 39]. Our gas phase data are consistent in that the biggest conformational change is caused by calcium coordination. Metal ions are indispensable for the interaction of protein-heparin complexes, thus it may be that important conformational changes are required for biological activity [16, 81, 82]. Measuring CCS of metal ion coordinated octasaccharide-protein complexes will help us further understand these processes.

Conclusions

We have shown that various metal ions induce a conformation contraction in heparin octasaccharide structure. This observation suggests a conformational change of heparin induced by metal ions may alter the interactions of heparin and heparin-binding proteins [18]. We have shown that the effects of metal coordination were more pronounced in lower charge state ions. Furthermore, we have shown that the number of metal ion adducts, the ionic radii, and the ionic valence of metal ions are all factors in metal-induced compact octasaccharide conformational change. There was little difference in the measurements of conformational change measured here in the gas phase with those of previous in solution measurements [20, 39]. For transition metal ions, the spin state of the ions has an effect on ionic radii. Given the different CCS measurements of metal ion-coordinated octasaccharides, our results may warrant future investigations into the structure-function relationships of other macromolecular structures.

Supplementary Material

Refer to Web version on PubMed Central for supplementary material.

Acknowledgments

We gratefully acknowledge Professor Michael T. Bowers (UC Santa Barbara, CA, USA), for the collision cross section measurements of the oligonucleotides. We also acknowledge NIH #GM47356 and NSF #CHE0909743 for supporting this research.

References

1. Jin L, Abrahams JP, Skinner R, Petitou M, Pike RN, Carrell RW. The anticoagulant activation of antithrombin by heparin. Proc Natl Acad Sci U S A. 1997; 94:14683–14688. [PubMed: 9405673]
2. Bernfield M, Gotte M, Park PW, Reizes O, Fitzgerald ML, Lincecum J, Zako M. Functions of cell surface heparan sulfate proteoglycans. Annu Rev Biochem. 1999; 68:729–777. [PubMed: 10872465]
3. Varki, A. Essentials of glycobiology. 2. Cold Spring Harbor Laboratory Press; Cold Spring Harbor, N.Y: 2009.
4. Gandhi NS, Mancera RL. The structure of glycosaminoglycans and their interactions with proteins. Chem Biol Drug Des. 2008; 72:455–482. [PubMed: 19090915]
5. Powell AK, Yates EA, Fernig DG, Turnbull JE. Interactions of heparin/heparan sulfate with proteins: Appraisal of structural factors and epxerimental approaches. Glycobiology. 2004; 14:17r–30r.
6. Ferro DR, Provasoli A, Ragazzi M, Casu B, Torri G, Bossennec V, Perly B, Sinay P, Petitou M, Choay J. Conformer populations of L-iduronic acid residues in glycosaminoglycan sequences. Carbohyd Res. 1990; 195:157–167.
7. Desai UR, Wang HM, Kelly TR, Linhardt RJ. Structure Elucidation of a Novel Acidic Tetrasaccharide and Hexasaccharide Derived from a Chemically Modified Heparin. Carbohyd Res. 1993; 241:249–259.
8. Ferro DR, Provasoli A, Ragazzi M, Torri G, Casu B, Gatti G, Jacquinet JC, Sinay P, Petitou M, Choay J. Evidence for Conformational Equilibrium of the Sulfated L-Iduronate Residue in Heparin and in Synthetic Heparin Monosaccharides and Oligosaccharides - Nmr and Force-Field Studies. J Am Chem Soc. 1986; 108:6773–6778.
9. Yates EA, Santini F, Guerrini M, Naggi A, Torri G, Casu B. H-1 and C-13 NMR spectral assignments of the major sequences of twelve systematically modified heparin derivatives. Carbohyd Res. 1996; 294:15–27.
10. Yates EA, Santini F, De Cristofano B, Payre N, Cosentino C, Guerrini M, Naggi A, Torri G, Hricovini M. Effect of substitution pattern on H-1, C-13 NMR chemical shifts and (1)J(CH) coupling constants in heparin derivatives. Carbohyd Res. 2000; 329:239–247.
11. Angulo J, Nieto PM, Martin-Lomas M. A molecular dynamics description of the conformational flexibility of the L-iduronate ring in glycosaminoglycans. Chem Commun. 2003:1512–1513.
12. Hricovíni, M.; Nieto, PM.; Torri, G. NMR of Sulfated Oligo- and Polysaccharides. In: Jiménez-Barbero, J.; Peters, T., editors. NMR Spectroscopy of Glycoconjugates. Wiley-VCH Verlag GmbH & Co. KGaA; Weinheim, FRG: 2003.
13. Capila I, Linhardt RJ. Heparin - Protein interactions. Angew Chem Int Edit. 2002; 41:391–412.
14. Conrad, HE. Heparin-binding proteins. Academic Press; San Diego: 1998.
15. Grootenhuis PDJ, Westerduin P, Meuleman D, Petitou M, Vanboeckel CAA. Rational Design of Synthetic Heparin Analogs with Tailor-Made Coagulation-Factor Inhibitory Activity. Nat Struct Biol. 1995; 2:736–739. [PubMed: 7552742]
16. Petitou M, van Boeckel CAA. A synthetic antithrombin III binding pentasaccharide is now a drug! What comes next? Angew Chem Int Edit. 2004; 43:3118–3133.
17. Kan M, Wang F, Xu J, Crabb JW, Hou J, McKeehan WL. An essential heparin-binding domain in the fibroblast growth factor receptor kinase. Science. 1993; 259:1918–1921. [PubMed: 8456318]

18. Capila I, Hernaiz MJ, Mo YD, Mealy TR, Campos B, Dedman JR, Linhardt RJ, Seaton BA. Annexin V--heparin oligosaccharide complex suggests heparan sulfate--mediated assembly on cell surfaces. Structure. 2001; 9:57–64. [PubMed: 11342135]
19. Manning GS. Counterion Binding in Polyelectrolyte Theory. Accounts Chem Res. 1979; 12:443–449.
20. Rabenstein DL, Robert JM, Peng J. Multinuclear magnetic resonance studies of the interaction of inorganic cations with heparin. Carbohyd Res. 1995; 278:239–256.
21. Ricard-Blum S, Feraud O, Lortat-Jacob H, Rencurosi A, Fukai N, Dkhissi F, Vittet D, Imberty A, Olsen BR, van der Rest M. Characterization of endostatin binding to heparin and heparan sulfate by surface plasmon resonance and molecular modeling: role of divalent cations. J Biol Chem. 2004; 279:2927–2936. [PubMed: 14585835]
22. Shao C, Zhang F, Kemp MM, Linhardt RJ, Waisman DM, Head JF, Seaton BA. Crystallographic analysis of calcium-dependent heparin binding to annexin A2. J Biol Chem. 2006; 281:31689–31695. [PubMed: 16882661]
23. Lages B, Stivala SS. Interaction of Polyelectrolyte Heparin with Copper(Ii) and Calcium. Biopolymers. 1973; 12:127–143. [PubMed: 4687142]
24. Chevalier F, Lucas R, Angulo J, Martin-Lomas M, Nieto PM. The heparin-Ca(2+) interaction: the influence of the O-sulfation pattern on binding. Carbohyd Res. 2004; 339:975–983.
25. Chevalier F, Angulo J, Lucas R, Nieto PM, Martin-Lomas M. The heparin-Ca2+ interaction: Structure of the Ca2+ binding site. Eur J Org Chem. 2002:2367–2376.
26. Gonzalez-Iglesias R, Pajares MA, Ocal C, Espinosa JC, Oesch B, Gasset M. Prion protein interaction with glycosaminoglycan occurs with the formation of oligomeric complexes stabilized by Cu(II) bridges. J Mol Biol. 2002; 319:527–540. [PubMed: 12051926]
27. Parrish RF, Fair WR. Selective binding of zinc ions to heparin rather than to other glycosaminoglycans. Biochem J. 1981; 193:407–410. [PubMed: 6796046]
28. Srinivasan SR, Radhakrishnamurthy B, Berenson GS. Studies on Interaction of Heparin with Serum-Lipoproteins in Presence of Ca2+, Mg2+, and Mn2+ Arch Biochem Biophys. 1975; 170:334–340. [PubMed: 169748]
29. Grant D, Long WF, Williamson FB. Infrared-Spectroscopy of Heparin Cation Complexes. Biochem J. 1987; 244:143–149. [PubMed: 3663108]
30. Grant D, Long WF, Moffat CF, Williamson FB. Infrared-Spectroscopy of Heparins Suggests That the Region 750–950 Cm-1 Is Sensitive to Changes in Iduronate Residue Ring Conformation. Biochem J. 1991; 275:193–197. [PubMed: 2018474]
31. Martin-Lomas M, Nieto PM, Khiar N, Garcia S, Flores-Mosquera M, Poirot E, Angulo J, Munoz JL. The solution conformation of glycosyl inositols related to inositolphosphoglycan (IPG) mediators. Tetrahedron-Asymmetr. 2000; 11:37–51.
32. Chevalier F, Lucas R, Angulo J, Martin-Lomas M, Nieto PM. The heparin-Ca2+ interaction: the influence of the O-sulfation pattern on binding. Carbohyd Res. 2004; 339:975–983.
33. Mulloy B, Forster MJ, Jones C, Davies DB. Nmr and Molecular-Modeling Studies of the Solution Conformation of Heparin. Biochem J. 1993; 293:849–858. [PubMed: 8352752]
34. Morris ER, Rees DA, Sanderson GR, Thom D. Conformation and Circular-Dichroism of Uronic Acid Residues in Glycosides and Polysaccharides. J Chem Soc Perk T. 1975; 2:1418–1425.
35. Buffington LA, Pysh ES, Chakrabarti B, Balazs EA. Far Uv Circular-Dichroism of N-Acetylglucosamine, Glucuronic Acid, and Hyaluronic-Acid. J Am Chem Soc. 1977; 99:1730–1734. [PubMed: 557067]
36. Villanueva GB, Allen N. Effect of Heparin Modification on Its Circular-Dichroism Spectrum. Biochem Bioph Res Co. 1984; 123:973–980.
37. Grant D, Long WF, Moffat CF, Williamson FB. Cu2+-Heparin Interaction Studied by Polarimetry. Biochem J. 1992; 283:243–246. [PubMed: 1567372]
38. Wallace BA. Conformational changes by synchrotron radiation circular dichroism spectroscopy. Nat Struct Biol. 2000; 7:708–709. [PubMed: 10966632]
39. Rudd TR, Guimond SE, Skidmore MA, Duchesne L, Guerrini M, Torri G, Cosentino C, Brown A, Clarke DT, Turnbull JE, Fernig DG, Yates EA. Influence of substitution pattern and cation binding

on conformation and activity in heparin derivatives. Glycobiology. 2007; 17:983–993. [PubMed: 17580314]

40. von Helden G, Wyttenbach T, Bowers MT. Conformation of Macromolecules in the Gas Phase: Use of Matrix-Assisted Laser Desorption Methods in Ion Chromatography. Science. 1995; 267:1483–1485. [PubMed: 17743549]
41. Ruotolo BT, Benesch JL, Sandercock AM, Hyung SJ, Robinson CV. Ion mobility-mass spectrometry analysis of large protein complexes. Nat Protoc. 2008; 3:1139–1152. [PubMed: 18600219]
42. Schenauer MR, Leary JA. An ion mobility-mass spectrometry investigation of monocyte chemoattractant protein-1. Int J Mass Spectrom. 2009; 287:70–76. [PubMed: 20160907]
43. Pringle SD, Giles K, Wildgoose JL, Williams JP, Slade SE, Thalassinos K, Bateman RH, Bowers MT, Scrivens JH. An investigation of the mobility separation of some peptide and protein ions using a new hybrid quadrupole/travelling wave IMS/oa-ToF instrument. Int J Mass Spectrom. 2007; 261:1–12.
44. Smith DP, Knapman TW, Campuzano I, Malham RW, Berryman JT, Radford SE, Ashcroft AE. Deciphering drift time measurements from travelling wave ion mobility spectrometry-mass spectrometry studies. Eur J Mass Spectrom. 2009; 15:113–130.
45. Shelimov KB, Clemmer DE, Hudgins RR, Jarrold MF. Protein structure in vacuo: Gas-phase confirmations of BPTI and cytochrome c. J Am Chem Soc. 1997; 119:2240–2248.
46. Myung S, Badman ER, Lee YJ, Clemmer DE. Structural transitions of electrosprayed ubiquitin ions stored in an ion trap over similar to 10 ms to 30 s. J Phys Chem A. 2002; 106:9976–9982.
47. Shelimov KB, Jarrold MF. Conformations, unfolding, and refolding of apomyoglobin in vacuum: An activation barrier for gas-phase protein folding. J Am Chem Soc. 1997; 119:2987–2994.
48. Scarff CA, Thalassinos K, Hilton GR, Scrivens JH. Travelling wave ion mobility mass spectrometry studies of protein structure: biological significance and comparison with X-ray crystallography and nuclear magnetic resonance spectroscopy measurements. Rapid Commun Mass Spectrom. 2008; 22:3297–3304. [PubMed: 18816489]
49. Jin L, Barran PE, Deakin JA, Lyon M, Uhrin D. Conformation of glycosaminoglycans by ion mobility mass spectrometry and molecular modelling. Phys Chem Chem Phys. 2005; 7:3464–3471. [PubMed: 16273147]
50. Thalassinos K, Grabenauer M, Slade SE, Hilton GR, Bowers MT, Scrivens JH. Characterization of Phosphorylated Peptides Using Traveling Wave-Based and Drift Cell Ion Mobility Mass Spectrometry. Anal Chem. 2009; 81:248–254. [PubMed: 19117454]
51. Leary JA, Schenauer MR, Stefanescu R, Andaya A, Ruotolo BT, Robinson CV, Thalassinos K, Scrivens JH, Sokabe M, Hershey JWB. Methodology for Measuring Conformation of Solvent-Disrupted Protein Subunits using T-WAVE Ion Mobility MS: An Investigation into Eukaryotic Initiation Factors. J Am Soc Mass Spectrom. 2009; 20:1699–1706. [PubMed: 19564121]
52. Liu YS, Clemmer DE. Characterizing oligosaccharides using injected-ion mobility mass spectrometry. Anal Chem. 1997; 69:2504–2509. [PubMed: 21639386]
53. Lee DS, Wu C, Hill HH. Detection of carbohydrates by electrospray ionization ion mobility spectrometry following microbore high-performance liquid chromatography. J Chromatogr A. 1998; 822:1–9.
54. Clowers BH, Dwivedi P, Steiner WE, Hill HH, Bendiak B. Separation of sodiated isobaric disaccharides and trisaccharides using electrospray ionization-atmospheric pressure ion mobility-time of flight mass spectrometry. J Am Soc Mass Spectrom. 2005; 16:660–669. [PubMed: 15862767]
55. Schenauer MR, Meissen JK, Seo Y, Ames JB, Leary JA. Heparan Sulfate Separation, Sequencing, and Isomeric Differentiation: Ion Mobility Spectrometry Reveals Specific Iduronic and Glucuronic Acid-Containing Hexasaccharides. Anal Chem. 2009; 81:10179–10185. [PubMed: 19925012]
56. Lee S, Wyttenbach T, Vonhelden G, Bowers MT. Gas-Phase Conformations of Li+, Na+, K+, and Cs+ Complexed with 18-Crown-6. J Am Chem Soc. 1995; 117:10159–10160.
57. Plasencia MD, Isailovic D, Merenbloom SI, Mechref Y, Clemmer DE. Resolving and Assigning N-Linked Glycan Structural Isomers from Ovalbumin by IMS-MS. J Am Soc Mass Spectrom. 2008; 19:1706–1715. [PubMed: 18760624]

58. Ototani N, Yosizawa Z. Anticoagulant activity of heparin octasaccharide. J Biochem. 1981; 90:1553–1556. [PubMed: 7338523]
59. Lindahl U, Backstrom G, Thunberg L, Leder IG. Evidence for a 3-O-sulfated D-glucosamine residue in the antithrombin-binding sequence of heparin. Proc Natl Acad Sci U S A. 1980; 77:6551–6555. [PubMed: 6935668]
60. Riesenfeld J, Thunberg L, Hook M, Lindahl U. The antithrombin-binding sequence of heparin. Location of essential N-sulfate groups. J Biol Chem. 1981; 256:2389–2394. [PubMed: 7462246]
61. Hasan J, Shnyder SD, Clamp AR, McGown AT, Bicknell R, Presta M, Bibby M, Double J, Craig S, Leeming D, Stevenson K, Gallagher JT, Jayson GC. Heparin octasaccharides inhibit angiogenesis in vivo. Clin Cancer Res. 2005; 11:8172–8179. [PubMed: 16299249]
62. Proudfoot AE, Handel TM, Johnson Z, Lau EK, LiWang P, Clark-Lewis I, Borlat F, Wells TN, Kosco-Vilbois MH. Glycosaminoglycan binding and oligomerization are essential for the in vivo activity of certain chemokines. Proc Natl Acad Sci U S A. 2003; 100:1885–1890. [PubMed: 12571364]
63. Lau EK, Paavola CD, Johnson Z, Gaudry JP, Geretti E, Borlat F, Kungl AJ, Proudfoot AE, Handel TM. Identification of the glycosaminoglycan binding site of the CC chemokine, MCP-1: implications for structure and function in vivo. J Biol Chem. 2004; 279:22294–22305. [PubMed: 15033992]
64. Schenauer MR, Meissen JK, Seo Y, Ames JB, Leary JA. Heparan Sulfate Separation, Sequencing, and Isomeric Differentiation: Ion Mobility Spectrometry Reveals Specific Iduronic and Glucuronic Acid-Containing Hexasaccharides. Anal Chem. 2009
65. Ruotolo BT, Giles K, Campuzano I, Sandercock AM, Bateman RH, Robinson CV. Evidence for macromolecular protein rings in the absence of bulk water. Science. 2005; 310:1658–1661. [PubMed: 16293722]
66. Williams JP, Scrivens JH. Coupling desorption electrospray ionisation and neutral desorption/extractive electrospray ionisation with a travelling-wave based ion mobility mass spectrometer for the analysis of drugs. Rapid Commun Mass Spectrom. 2008; 22:187–196. [PubMed: 18069748]
67. Remko M, von der Lieth CW. Gas-phase and solution conformations of selected dimeric structural units of heparin. J Chem Inf Model. 2006; 46:1687–1694. [PubMed: 16859300]
68. Capila I, Hernaiz MJ, Mo YD, Mealy TR, Campos B, Dedman JR, Linhardt RJ, Seaton BA. Annexin V-heparin oligosaccharide complex suggests heparan sulfate-mediated assembly on cell surfaces. Structure. 2001; 9:57–64. [PubMed: 11342135]
69. Eckert R, Ragg H. Zinc ions promote the interaction between heparin and heparin cofactor II. Febs Letters. 2003; 541:121–125. [PubMed: 12706831]
70. Templeton DM, Sarkar B. Peptide and Carbohydrate Complexes of Nickel in Human-Kidney. Biochem J. 1985; 230:35–42. [PubMed: 4052044]
71. Leavell MD, Gaucher SP, Leary JA, Taraszka JA, Clemmer DE. Conformational studies of Zn-ligand-hexose diastereomers using ion mobility measurements and density functional theory calculations. J Am Soc Mass Spectrom. 2002; 13:284–293. [PubMed: 11908808]
72. Leavell MD, Leary JA. Stabilization and linkage analysis of metal-ligated sialic acid containing oligosaccharides. J Am Soc Mass Spectrom. 2001; 12:528–536. [PubMed: 11349950]
73. Sible EM, Brimmer SP, Leary JA. Interaction of first row transition metals with alpha 1–3, alpha 1–6 mannotriose and conserved trimannosyl core oligosaccharides: A comparative electrospray ionization study of doubly and singly charged complexes. J Am Soc Mass Spectrom. 1997; 8:32–42.
74. Zheng YJ, Ornstein RL, Leary JA. A density functional theory investigation of metal ion binding sites in monosaccharides. J Mol Struc-Theochem. 1997; 389:233–240.
75. Fura A, Leary JA. Differentiation of Ca(2+)- and Mg(2+)-coordinated branched trisaccharide isomers: an electrospray ionization and tandem mass spectrometry study. Anal Chem. 1993; 65:2805–2811. [PubMed: 8250263]
76. Scarff CA, Thalassinos K, Hilton GR, Scrivens JH. Travelling wave ion mobility mass spectrometry studies of protein structure: biological significance and comparison with X-ray crystallography and nuclear magnetic resonance spectroscopy measurements. Rapid Commun Mass Spectrom. 2008; 22:3297–3304. [PubMed: 18816489]

77. Thalassinos K, Grabenauer M, Slade SE, Hilton GR, Bowers MT, Scrivens JH. Characterization of phosphorylated peptides using traveling wave-based and drift cell ion mobility mass spectrometry. Anal Chem. 2009; 81:248–254. [PubMed: 19117454]

78. Hensley P, Edelstein SJ, Wharton DC, Gibson QH. Conformation and Spin State in Methemoglobin. J Biol Chem. 1975; 250:952–960. [PubMed: 234444]

79. Hoard JL, Hamor MJ, Hamor TA, Caughey WS. Crystal Structure and Molecular Stereochemistry of Methoxyiron(3) Mesoporphyrin-9 Dimethyl Ester. J Am Chem Soc. 1965; 87:2312.

80. Hoard JL. Stereochemistry of hemes and other metalloporphyrins. Science. 1971; 174:1295–1302. [PubMed: 4332625]

81. Vanboeckel CAA, Grootenhuis PDJ, Visser A. A Mechanism for Heparin-Induced Potentiation of Antithrombin-Iii. Nat Struct Biol. 1994; 1:423–425. [PubMed: 7664058]

82. Guerrini M, Guglieri S, Beccati D, Torri G, Viskov C, Mourier P. Conformational transitions induced in heparin octasaccharides by binding with antithrombin III. Biochem J. 2006; 399:191–198. [PubMed: 16796563]

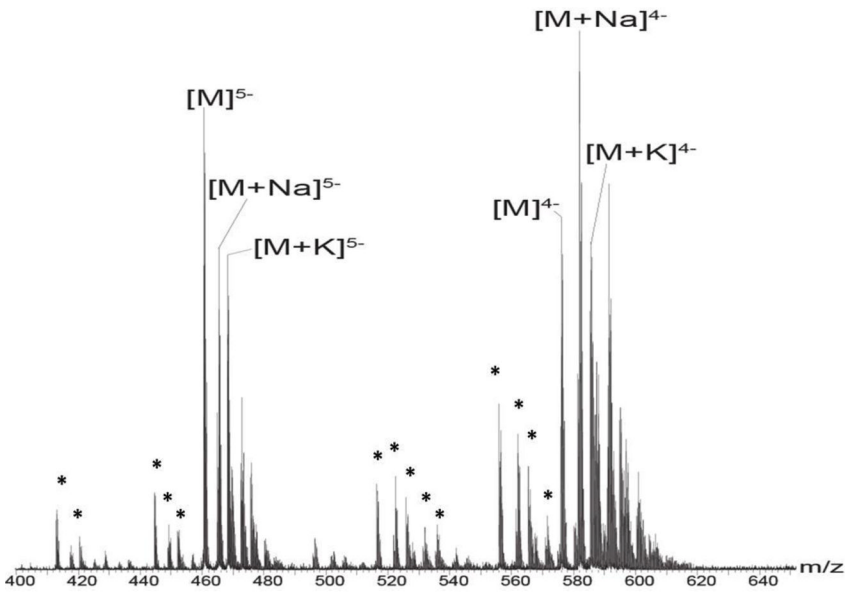

Figure 1.

Negative ion mode mass spectrum of 10μM dodecasulfated heparin octasaccharide dissolved in menthol/water/acetic acid solution (49/49/2; v/v/v). M represents dodecasulfated heparin octasaccharide. The charge distributions of 4- and 5- ions of heparin octasaccharides are illustrated. Asterisks represent desulfated ions corresponding to 5- or 4- charge state species. Mass to charge ratios of the heparin octasaccharides are shown in Table 1 of supplementary material.

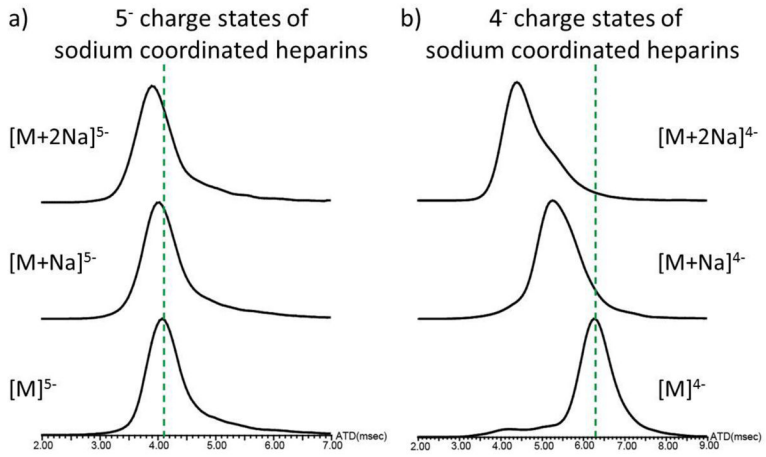

Figure 2.

The arrival time distributions for sodium coordinated heparin octasaccharide a) in the 5- charge state and b) in the 4- charge state. The dash lines indicate the baseline of the arrival time distribution for sodium-free coordinated heparin octasaccharide. Arrival time distributions are recorded in milliseconds.

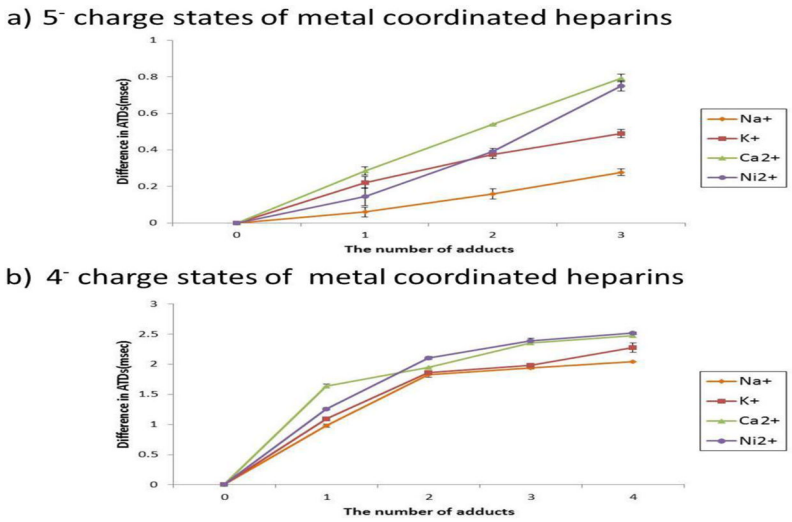

Figure 3.

The difference in arrival time distributions between metal and metal free coordinated heparin octasaccharide, plotted against the number of metal adducts a) in the 5- charge state b) in the 4- charge state. Differences in ATDs are calculated by subtracting the ATDs for metal coordinated octasaccharides from those of the metal free species. ATDs of calcium and potassium coordinated octasaccharide that exhibit two ion populations in the ion mobility spectrum are shown with the most abundant ion population represented.

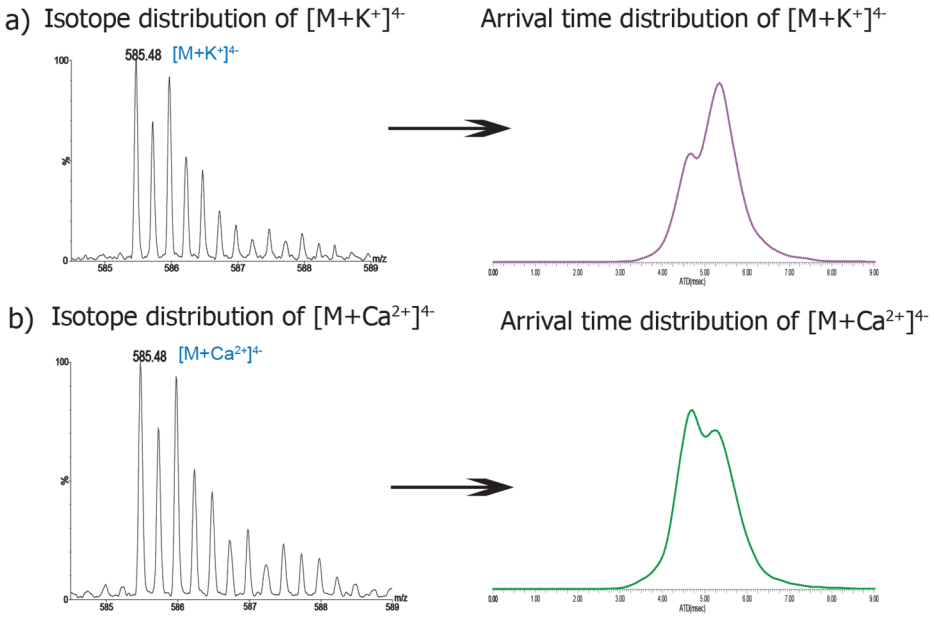

Figure 4.

Isotope distributions and arrival time distributions of heparin octasaccharide bound to a) one potassium ion b) and one calcium ion. The theoretical monoisotope mass difference is 2.2 mDa between K^+ and Ca^{2+}. There are two slightly different ion populations corresponding to K^+- and Ca^{2+}-coordinated octasaccharide in the ion mobility spectrum.

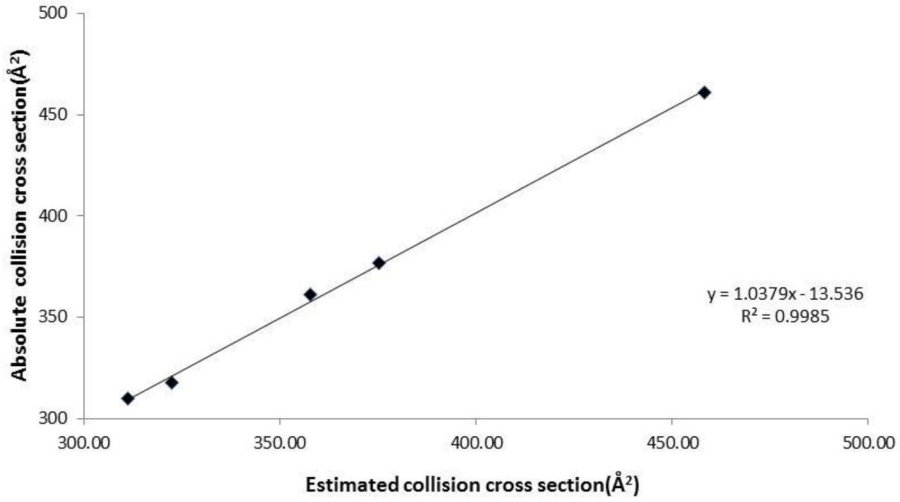

Figure 5.
The relationship between estimated and absolute collision cross sections using linear fit calibration.

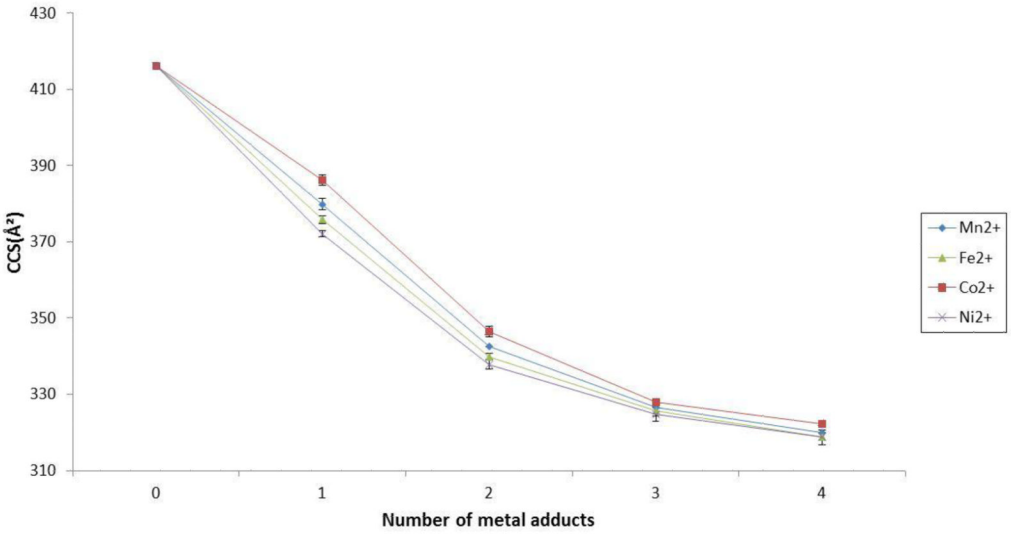

Figure 6.

Collision cross sections ($Å^2$) of transition metal coordinated octasaccharides plotted against the number of transition metal adducts in the 4^- charge state.

Table 1

Collision cross sections of alkali and alkaline earth metal coordinated heparin octasaccharide in the 4^- charge state. Either one potassium or one calcium coordinated octasaccharide shows two collision cross sections resulting from ATDs with two ion populations in the ion mobility spectrum. The data are from five individual measurements.

a) Alkali metal coordination		
# of adduct	Na^+	K^+
	CCS(Å^2)	CCS(Å^2)
0	413.22 ± 0.00	413.22 ± 0.00
1	381.08 ± 0.90	377.45 ± 0.00
		358.12 ± 0.00
2	353.20 ± 1.47	352.18 ± 0.00
3	349.56 ± 0.73	348.39 ± 0.72
4	346.26 ± 0.00	338.52 ± 2.64

b) Alkaline earth metal coordination		
# of adduct	Mg^{2+}	Ca^{2+}
	CCS(Å^2)	CCS(Å^2)
0	413.22 ± 0.00	413.22 ± 0.00
1	376.17 ± 0.00	380.21 ± 2.37
		359.56 ± 1.22
2	347.63 ± 0.73	349.23 ± 0.00
3	342.49 ± 1.30	336.08 ± 0.00
4	335.39 ± 1.34	332.10 ±0.90

Table 2

Collision cross sections of transition metal coordinated heparin octasaccharide in the 4^- charge state. The data are from five individual measurements.

# of adduct	Mn^{2+}	Fe^{2+}	Co^{2+}	Ni^{2+}
	CCS(Å^2)	CCS(Å^2)	CCS(Å^2)	CCS(Å^2)
0	413.22 ± 0.00	413.22 ± 0.00	413.22 ± 0.00	413.22 ± 0.00
1	378.68 ± 1.26	375.14 ± 0.90	384.38 ± 1.32	371.86 ± 0.73
2	347.88 ± 0.00	345.72 ± 0.72	350.75 ± 1.05	344.27 ± 0.90
3	336.02 ± 0.00	335.37 ± 0.90	337.05 ± 0.59	334.77 ± 1.26
4	331.3 ± 0.00	330.53 ± 1.30	332.99 ± 0.00	330.57 ± 0.72